Nature of polar state in 0.67BiFeO3–0.33BaTiO3

Yongxing Wei (weiyx1985@gmail.com)
Xi'an Technological University https://orcid.org/0000-0003-4509-8518
JIAHAO SHEN
Xi'an Technological University
CHENXING BAI
Xi'an Technological University
CHANGQING JIN
Xi'an Technological University
WEITONG ZHU
Xi'an Jiaotong University
YE TIAN
Shaanxi University of Science and Technology
GANG XU
Xi'an Technological University

Research Article

Keywords: lead-free; BiFeO3; MPB; pseudocubic structure; piezoelectric

Posted Date: May 11th, 2020

DOI: https://doi.org/10.21203/rs.3.rs-27129/v1

Version of Record: A version of this preprint was published at Journal of Materials Science: Materials in Electronics on September 22nd, 2020. See the published version at https://doi.org/10.1007/s10854-020-04462-9.

Abstract

This study was conducted to further understand the nature of the polar state in 0.67BiFeO3–0.33BaTiO3 (0.67BF–0.33BT). A typical relaxor-type dielectric anomaly was observed (Tf = ~627 K, TB = ~820 K). The remnant polarization (Pr), maximum value of electrostrain (Sm) and magnitude strain at Ec in the bipolar mode (Sneg) increase clearly during heating (Pr, ~40 mC/cm2; Sm, 0.191 % under 40 kV/cm at 453 K). The first-cycle bipolar electrostrain loops indicate that the minimum strain on the negative side of the bipolar strain curves is negative. The slopes of the relative permittivity versus log frequency plots in unpoled (–21) and poled (–23) specimens are similar. The transition between the ergodic relaxor state and ferroelectric-like state does not involve a clear dielectric anomaly even in the poled specimen. Analyses based on the Rietveld refinement of XRD patterns, bright-field images and selected-area electron diffractions (SAED) demonstrate that the formation of the long-range ferroelectric domains is difficult under the poling field.

1 Introduction

$BiFeO_3$–$BaTiO_3$ (BF–BT), first reported by Ismailzade et al. in 1981 [1], aroused great interest because of its multiferroic properties in the initial stage [2–4]. In 2009, the good piezoelectric coefficient (d_{33}, 116 pC/N) and high Curie temperature (T_c, > 873 K) of 0.75BF–0.25BT were obtained by the Mn modification [5]. The studies by Wei et al. and Yang et al. confirmed that the optimum piezoelectric properties were realized in compositions ($BaTiO_3$ content, ~ 30 mol%) near the morphotropic phase boundary (MPB) [6–8]. In 2015, the high piezoelectric performance (d_{33}, 402 pC/N) and large electrostrain (S_m, ~ 0.2% under 50 kV/cm) were reported in the water quenched BF–BT ceramics [9]. Advanced with the high depolarization temperature (T_d, > 673 K) and good thermal stability, BF–BT has become one of the most promising lead-free options [10–24].

Despite the intensive studies, the controversy on the origin of MPB has continued. The early study suggested a cubic phase appeared when the $BaTiO_3$ content reached 33 mol% [1, 2]. Leontsev et al. held that the $BaTiO_3$-rich phase should be pesudocubic due to the presence of the ferroelectric and piezoelectric properties [3]. The study by Lee et al. highlighted the similarity in MPB between BF–BT and $Pb(Zr,Ti)O_3$ [9]. In 2017, Wang et al. found that the electrostrain of 0.7BF–0.3BT increased when heated [13]. A field induced relaxor-ferroelectric transition was presumed to interpret this enhancement. However, the in-situ synchrotron X–ray diffraction (XRD) in combination with Rietveld refinement of pseudocubic BF–BT suggested that there was no clear peak splitting when the poling field was imposed [20, 21].

Is the initial state of 0.67BF–0.33BT (a) a nonergodic relaxor state that develops to a long-range ferroelectric state under the electric field, (b) a ferroelectric state with small tetragonal distortion, (c) or a ferroelectric state with nanodomains adopted pseudocubic symmetry on the global length scale? The structure changes based on the above three models are too similar to be resolved by X-ray diffractions. The analyses of the first-cycle electrostrain loop and structure-property relationship of the poled sample

are important. If the transition from the nonergodic relaxor state to the ferroelectric state occurs, we could observe its effect on the first-cycle electrostrain loop, domain structure and dielectric properties like $Bi_{0.5}Na_{0.5}TiO_3$-based ceramics [25–28]. In this study, temperature dependence of dielectric behaviors, polarization responses and electrostrain responses, the initial electrostrain loops and poling effects on the structural and electrical properties of 0.67BF–0.33BT were analyzed to understand its polar state. MnO_2 was introduced to reduce the conduction effects on the high-temperature electrical properties [3, 29].

2 Experimental

Solid solution ceramics of 0.67BF–0.33BT were prepared by the solid-state reaction method, with the starting reagents of Bi_2O_3, $BaCO_3$, Fe_2O_3 and TiO_2. 1 mol% MnO_2 was added. The sintering temperature was 1000 ^oC. For the electrical measurements, the silver paste was coated and fired at 550 °C for 10 minutes. The dielectric data were measured using an LCR meter (4294 A, Agilent, Santa Clara, America) with a temperature-controlled cell. The ferroelectric properties and the electrostrain responses at 1 Hz were measured using a ferroelectric test system (TF Analyzer 2000E, aixACCT, Aachen, Germany). The ceramics were poled in the silicone oil for 10 minutes under a dc field of 40 kV/cm at 298 K for the piezoelectric measurement. The piezoelectric coefficients (d_{33}) were measured using a piezo-d_{33} meter (ZJ–3AN; Institute of Acoustics, Beijing, China). The crystal structures were detected using an X–ray diffractometer (XRD, D2 PHASER, Bruker AXS, Karlsruhe, Germany). The Rietveld refinement analysis (using the FullProf software) was performed to study the poling effect on the structure. The bright-field images and selected-area electron diffraction SAED patterns were obtained by the transmission electron microscopy (TEM, JEM-2100Plus; JEOL, Okyo Metropolis, Japan). Before TEM observation, the unpoled and poled specimens were prepared by polishing, dimpling and ion milling.

3. Results And Discussion

Figure 1(a) shows the relative permittivity (ε_r) and dielectric loss ($tan\delta$) of 0.67BF–0.33BT as a function of temperature at various frequencies. The composition shows a relaxor-like dielectric anomaly in the temperature range between 650 K and 750 K. Benefitting from high insulation by Mn modification, the dielectric anomaly at 100 Hz could be clearly observed [8]. The relationship between the temperature (T_m) for the maximum value of ε_r and measuring frequency can be well described by the Vogel-Fulcher law (Fig. 1b) [30], giving a freezing temperature (T_f) of ~ 627 K, ~ 50 K higher than that reported by Zheng et al. [11]. The relationship between the piezoelectric coefficient (d_{33}) and annealing temperature indicates that the depolarization temperature is ~ 650 K, close to T_f (Fig. 1c). Above 800 K, there is a clear increase in the relative permittivity at 100 Hz and 1 kHz. This should be related to the thermally excited charge carriers. In relaxor ferroelectrics, the polar nano regions (PNRs) appear at the Burns temperature (T_B) where the relationship between the reciprocal permittivity and temperature departs from the Curie-Weiss law when cooled [30]. The high temperature data at 100 kHz, which are less effected by conductivity, were

used to define the T_B value (Fig. 1d). The T_B value was found to be ~ 820 K, ~ 95 K higher than T_m (725 K at 100 kHz). The Curie parameters T_{CW} and C are ~ 746 K and ~ $1.22 \cdot 10^6$ K, respectively.

The polarization and electro-strain responses during heating were studied to better understand the ferroelectric-like state of 0.67BF–0.33BT (Fig. 2a–c). The detailed experimental results are shown in Fig. S1 in the supporting information. The remnant polarization (P_r) increases clearly with the temperature, accompanied by a reduction in the coercive field (E_c). Above 398 K, the conduction contributes much to the polarization response. We obtained the intrinsic ferroelectric hysteresis loop by deducting the conduction effect, assuming that the relation of leakage current density and electric field is linear [31]. The intrinsic P_r value of 0.67BF–0.33BT is ~ 40 μC/cm^2 at 453 K, much higher than that of $Bi_{0.5}Na_{0.5}TiO_3$(BNT) [27]. Most importantly, the heating also induces an enhancement of the electrostrain. At 453 K, the maximum value of unipolar strain (S_m) and large-signal piezoelectric coefficient (d_{33}^*) are ~ 0.191% and ~ 477 pm/V, respectively. The trends of the polarization and electrostrain for 0.67BF–0.33BT when heated are identical with those reported in 0.7BF–0.3BT [13, 32]. In addition, the magnitude strain at E_c in the bipolar mode (S_{neg}) increases from 0.07% at 300 K to 0.17% at 453 K. The finding hints that the heating activates more non-180^o domains switching [33].

The first-cycle electrostrain loops in BNT-based nonergodic relaxor materials exhibit two distinctive features [33], which hints the electric-filed-induced transition from the relaxor state to the ferroelectric state induced. (1) The strain increases abruptly above a certain threshold electric field. (2) The minimum strain on the negative side of the bipolar strain curve, which could be named as the “irrecoverable” strain (S_{irr}) [25], is positive. To further understand the initial state, the first-cycle ferroelectric hysteresis loop and electrostrain loop of 0.67BF–0.33BT were measured (Fig. 3). The composition shows a pronounced increase in the polarization and strain above E_c at room temperature (Fig. 3a). A ~ 0.04% remnant strain could be observed when the poling field was removed. Unlike BNT-based nonergodic relaxor ceramics [22, 25, 33, 34], the S_{irr} value of 0.67BF–0.33BT is negative. The sign of S_{irr} is unchanged when the measuring temperature is 453 K. The strain increases clearly when the electric field is imposed. The initial curve of strain and electric field was found to obey the following expression

$$S = aE + bE2,$$

where S is the strain, E is the electric field, and a (0.0036 ± 0.0001) and b (0.000110 ± 0.000006) are fitting parameters.

The poling effect on the relationship between the dielectric behavior and log frequency is plotted in Fig. 4. The low dielectric loss in a low frequency range suggests that the leakage current is effectively suppressed near the room temperature by Mn-modification. The relative permittivity of the unpoled sample is frequency dependent. In order to estimate the frequency dispersion, the slope of relative permittivity versus log frequency plots was calculated. The *slope* of the unpoled sample is approximately

− 21. After poling, the relative permittivity increases clearly but the frequency dispersion behaviors are nearly unchanged (*slope*, approximately − 23).

The temperature dependence of relative permittivity suggests that the T_m value shifts to the high-temperature side after poling (Fig. 5a). At 100 kHz, the poling leads to an increase of T_m from 725 K to 729 K. The increase in T_m by poling was also observed in $PbMg_{1/3}Nb_{2/3}O–PbTiO_3$ [35]. Most importantly, there is no clear dielectric anomaly related to the transition point between ferroelectric-like state and relaxor state in the poled specimen. The poling effect on the relationship between dielectric loss and temperature is shown in Fig. 5(b). The dielectric loss anomaly temperature also increases after poling. In addition, there is another loss anomaly at 500 kHz around 650 K. The anomaly point is corresponding to the depolarization temperature. This loss anomaly is only observed in the measuring frequency that is close to the resonant frequency. Therefore, it could be understood as the resonant effect due to poling.

The XRD patterns of unpoled and poled powdered specimens for 0.67BF–0.33BT are shown in Fig. 6(a) and (b). A cubic-like perovskite phase was found both in unpoled and poled specimens, consistent with the in-situ synchrotron radiation XRD analyses [20, 21]. The reflection peak shifts to the low-angle side after poling. Rietveld refine analysis suggests that the structures could be well described by the cubic symmetry with the space group of Pm_3m. The poling leads to a 0.14% increase in the lattice parameter (*a*). The increase in the lattice parameter by dc electric field poling is much larger than the observed remnant strain (~ 0.04%) (Fig. 3a).

The bright-field TEM images of many grains were examined to understand the micro polar order. No viable ferroelectric domains were detected both in the unpoled (Fig. 6c) and poled state (Fig. 6d). It reveals the difficulty in the formation of long-range ferroelectric domains under the poling field.

To further understand the poling effect on the structure, the SAED patterns with [110] zone axis were obtained (Fig. 6e and f). The absence of the super-lattice reflection spots $1/2(111)_c$ suggests that there is no ordered rotation of the octahedral both in the initial and poled state of 0.67BF–0.33BT [36]. That is, the R3c structure should be eliminated if the rombohedral distortions are present on the local scale. The increase in the tolerance factor (t = 0.968 for 0.75BF–0.25BT, t = 0.970 for $Bi_{1/2}Na_{1/2}TiO_3$ and t = 0.978 for 0.67BF–0.33BT) and the degree of disorder with increasing $BaTiO_3$ content leads to the difficulty in the ordered rotation of the octahedral.

We compared 0.67BF–0.33BT with $0.64PbMg_{1/3}Nb_{2/3}O_3–0.36PbTiO_3$ (0.64PMN–0.36PT) [37] and $0.94Bi_{1/2}Na_{1/2}TiO_3–0.06PbTiO_3$ (0.94BNT–0.06BT) [22, 23, 38–40] near MPB (Table 1) to better understand its structural and electrical characteristics. The eight main differences in 0.67BF–0.33BT are summarized as below.

(1) Both the structures of the unpoled and poled states could be well understood as the pseudocubic symmetry [20, 21].

(2) No visible ferroelectric domains could be detected in the unpoled state. The poling field hardly triggers the formation of the long-range ferroelectric domains.

(3) The frequency dispersion behavior is obvious in the unpoled specimen. Poling does not induce distinct change in the frequency dispersion behavior.

(4) The frequency dependence of T_m is obvious and well fitted by the V-F functions.

(5) The difference of T_m and T_B is about ~ 95 K, higher than that in 0.64PMN–0.36PT but lower than that in 0.94BNT–0.06BT.

(6) The relationship between the relative permittivity and temperature in the poled sample lacks the clear anomaly related to the transition from the relaxor state to the ferroelectric-like state.

(7) Different from typical nonergodic ralaxors, the initial electrostrain loops show a negative S_{irr}.

(8) The heating leads to an increase in P_r, S_m and S_{neg}, even the maximum measuring temperature is ~ 200 K lower than T_d.

Our studies reveal the complexity of 0.67BF–0.33BT. This is possibly caused by the mixtures of the ferroelectrically active and non-ferroelectrically active cations both on the A site and B site. We hope our study could promote the understanding in the polar state of 0.67BF–0.33BT.

4. Conclusions

The temperature dependence of dielectric properties of 0.67BF-0.33BT shows typical relaxor features, with T_f *and* T_B of ~ 627 K and ~ 820 K. P_r, S_m and S_{neg} increase with temperature. The intrinsic P_r reaches ~ 40 μC/cm^2 at 453 K. Unlike BNT-based nonergodic relaxor ceramics, the S_{irr} values in the initial strain loops at 300 K and 453 K are both negative. The poling does not lead a clear change in the frequency dispersion behaviors and peak splitting. The bright-field image of the poling sample suggests that the formation of the long-range domains is difficult when the poling field is imposed. Our studies indicate that there are distinct differences in the polar states among the MPB compositions of BF–BT, PMN–PT and BNT–BT. The local structures of 0.67BF–0.33BT remains unclear and should be further studied.

Supplementary Material

See supplementary material for the polarization, bipolar and unipolar strain responses at various temperatures (Fig. S1) of 0.67BF–0.33BT.

Declarations

Acknowledgements

This work was financially supported by the National Natural Science Foundation of China (Project No. 11704301), the Natural Science Basic Research Plan in Shaanxi Province of China (Program No. 2018JQ1092), the Shaanxi Provincial Education Department Program (Program No.19JK0398) and the President's Fund of Xi'an Technological University (Project no. XAGDXJJ18006).

Data sharing policy

The data that support the findings of this study are available from the corresponding author upon reasonable request.

References

1. Ismailzade IH, Ismailov RM, Alekberov AI, et al. Investigation of the magnetoelectric $(ME)_H$ effect in solid solutions of the systems $BiFeO_3$–$BaTiO_3$ and $BiFeO_3$–$PbTiO_3$. Phys Status Solidi (a). 1981;68:K81–5.
2. Kumar MM, Srinivas A, Suryanarayana SV. Structure property relations in $BiFeO_3$/$BaTiO_3$ solid solutions. J Appl Phys. 2000;87:855–62.
3. Kim JS, Cheon CI, Lee CH, et al. Weak ferromagnetism in the ferroelectric $BiFeO_3$–$ReFeO_3$–$BaTiO_3$ solid solutions (Re = Dy, La). J Appl Phys. 2004;96:468–74.
4. Singh A, Pandey V, Kotnala RK, et al. Direct Evidence for Multiferroic Magnetoelectric Coupling in $0.9BiFeO_3$–$0.1BaTiO_3$. Phys Rev Lett. 2008;101:247602.
5. Leontsev SO, Eitel RE. Dielectric and piezoelectric properties in Mn-modified $(1 – x)BiFeO_3$–$xBaTiO_3$ ceramics. J Am Ceram Soc. 2009;92:2957–61.
6. Wei YX, Wang XT, Jia JJ, et al. Multiferroic and piezoelectric properties of $0.65BiFeO_3$–$0.35BaTiO_3$ ceramic with pseudo-cubic symmetry. Ceram Int. 2012;38:3499–502.
7. Yang HB, Zhou CR, Liu XY, et al. Structural, microstructural and electrical properties of $BiFeO_3$–$BaTiO_3$ ceramics with high thermal stability. Mater Res Bull. 2012;47:4233–9.
8. Wei YX, Wang XT, Zhu JT, et al. Dielectric, ferroelectric, and piezoelectric properties of $BiFeO_3$-$BaTiO_3$ ceramics. J Am Ceram Soc. 2013;96:3163–8.
9. Lee MH, Kim DJ, Park JS, et al. High-performance lead-free piezoceramics with high Curie temperatures. Adv Mater. 2015;27:6976–82.
10. Zheng T, Jiang ZG, Wu JG. Enhanced piezoelectricity in $(1 – x)Bi_{1.05}Fe_{1-y}A_yO_3$–$xBaTiO_3$ lead-free ceramics: site engineering and wide phase boundary region. Dalton Trans. 2016;45:11277–85.
11. Zheng DG, Zuo RZ, Zhang DS, et al. Novel $BiFeO_3$–$BaTiO_3$–$Ba(Mg_{1/3}Nb_{2/3})O_3$ lead-free relaxor ferroelectric ceramics for energy-storage capacitors. J Am Ceram Soc. 2015;98:2692–5.

12. Zhang HL, Jo W, Wang K, et al. Compositional dependence of dielectric and ferroelectric properties in $BiFeO_3$–$BaTiO_3$ solid solutions. Ceram Int. 2014;40:4759–65.
13. Wang DW, Khesro A, Murakami S, et al. Temperature dependent, large electromechanical strain in Nd-doped $BiFeO_3$–$BaTiO_3$ lead-free ceramics. J Eur Ceram Soc. 2017;37:1857–60.
14. Chen JG, Chen JR. Enhanced thermal stability of lead-free high temperature $0.75BiFeO_3$–$0.25BaTiO_3$ ceramics with excess Bi content. J Alloy Compd. 2014;589:115–9.
15. Calisir I, Amirov AA, Kleppe AK, et al. Optimisation of functional properties in lead-free $BiFeO_3$–$BaTiO_3$ ceramics through La^{3+} substitution strategy. J Mater Chem A. 2018;6:5378 – 5397.
16. Xun BW, Wang N, Zhang BP, et al. Enhanced piezoelectric properties of $0.7BiFeO_3$–$0.3BaTiO_3$ lead-free piezoceramics with high Curie temperature by optimizing Bi self-compensation. Ceram Int. 2019;45:24382–91.
17. Wang L, Liang RH, Zhou ZY, et al. Thermally stable electrostrain in $BiFeO_3$–$BaTiO_3$-based high temperature lead-free piezoceramics. Appl Phys Lett. 2019;115:08202.
18. Liu X, Zhai JW, Shen B, et al. Novel bismuth ferrite-based lead-free incipient piezoceramics with high electromechanical response. J Mater Chem C. 2019;7:5122–30.
19. Wang DW, Wang G, Murakami S, et al. $BiFeO_3$–$BaTiO_3$: A new generation of lead-free electroceramics. J Adv Dielectr. 2018;8:1830004.
20. Kim S, Khanal GP, Nam HW, et al. In-situ electric field induced lattice strain response observation in $BiFeO_3$–$BaTiO_3$ lead-free piezoelectric ceramics. J Ceram Soc Jpn. 2018;126:316–20.
21. Wang G, Fan ZM, Murakami S, et al. Origin of the large electrostrain in $BiFeO_3$–$BaTiO_3$ based lead-free ceramics. J Mater Chem A. 2019;7:21254–63.
22. Paterson AR, Nagata H, Tan XL, et al. Relaxor-ferroelectric transitions: Sodium bismuth titanate derivatives. MRS Bull. 2018;43:600–6.
23. Gao JH, Ke XQ, Acosta M, et al. High piezoelectricity by multiphase coexisting point: Barium titanate derivatives. MRS Bull. 2018;43:595–9.
24. Wang K, Malic B, Wu JG, et al. Shifting the phase boundary: Potassium sodium niobate derivates. MRS Bull. 2018;43:607–11.
25. Jo W, Rodel J. Electric-field-induced volume change and room temperature phase stability of $(Bi_{1/2}Na_{1/2})TiO_3$-x mol. % $BaTiO_3$ piezoceramics. Appl Phys Lett. 2001;99:042901.
26. Jo W, Schaab S, Sapper E, et al. On the phase identity and its thermal evolution of lead free $(Bi_{1/2}Na_{1/2})TiO_3$-6 mol%$BaTiO_3$. J Appl Phys. 2011;110:074106.
27. Rao BN, Datta R, Chandrashekaran SS, et al. Local structural disorder and its influence on the average global structureand polar properties in $Na_{0.5}Bi_{0.5}TiO_3$. Rhys Rev B. 2013;88:224103.
28. Rao BN, Ranjan R. Electric-field-driven monoclinic-to-rhombohedral transformation in $Na_{1/2}Bi_{1/2}TiO_3$. Rhys Rev B. 2012;86:134103.

29. Li Q, Wei JX, Cheng JR, et al. High temperature dielectric, ferroelectric and piezoelectric properties of Mn-modified $BiFeO_3$-$BaTiO_3$ lead-free ceramics. J Mater Sci. 2017;52:229–37.
30. Bokov AA, Ye ZG. Recent progress in relaxor ferroelectrics with perovskite structure. J Mater Sci. 2006;41:31–52.
31. Yan HX, Inam F, Viola G, et al. The contribution of electrical conductivity, dielectric permittivity and domain switching in ferroelectric hysteresis loops. J Adv Dielectr. 2011;1:107–18.
32. Zhu LF, Liu Q, Zhang BP, et al. Temperature independence of piezoelectric properties for high-performance $BiFeO_3$–$BaTiO_3$ lead-free piezoelectric ceramics up to 300 °C. RSC Adv. 2018;8:35794–801.
33. Jo W, Dittmer R, Acosta M, et al. Giant electric-field-induced strains in lead-free ceramics for actuator applications–status and perspective. J Electroceram. 2012;29:71–93.
34. Yin J, Tao H, Liu G, et al. Domain-scale imaging to dispel the clouds over the thermal depolarization of $Bi_{0.5}Na_{0.5}TiO_3$-based relaxor ferroelectrics. J Am Ceram Soc. 2020;103:1881–90.
35. Sehirlioglu A, Payne DA, Han PD. Effect of poling on dielectric anomalies at phase transitions for lead magnesium niobate-lead titanate crystals in the morphotropic phase boundary region. J Appl Phys. 2006;99:064101.
36. Narayan B, Malhotra JS, Pandey R, et al. Electrostrain in excess of 1% in polycrystalline piezoelectrics. Nature Mater. 2017;17:427–31.
37. Li F, Zhang SJ, Damjanovic D, et al. Local structural heterogeneity and electromechanical responses of ferroelectrics: learning from relaxor ferroelectrics. Adv Funct Mater. 2018;28:1801514.
38. Maurya D, Pramanick A, Feygenson M, et al. Effect of poling on nanodomains and nanoscale structure in A-site disordered lead-free piezoelectric $Na_{0.5}Bi_{0.5}TiO_3$–$BaTiO_3$. J Mater Chem C. 2014;2:8423–31.
39. Zhao JY, Zhang N, Ren W, et al. Polar domain structural evolution under electric field and temperature in the $(Bi_{0.5}Na_{0.5})TiO_3$-0.06$BaTiO_3$ piezoceramics. J Am Ceram Soc. 2019;102:437–47.
40. Shi X, Kumar N, Hoffman M. Electric field–temperature phase diagrams for $(Bi_{1/2}Na_{1/2})TiO_3$–$BaTiO_3$–$(K_{1/2}Na_{1/2})NbO_3$ relaxor ceramics. J Mater Chem C. 2018;6:12224–33.

Tables

TABLE 1*. Structural and electrical characteristics of* 0.64PMN–0.36PT, 0.94BNT–0.06BT and 0.67BF–0.33BT. FE, ferroelectric.

Composition	0.64PMN-0.36PT[37]	0.94BNT-0.06BT[22,23,33–35]		0.67BF-0.33BT	
		unpoled	poled	unpoled	poled
Structure	Tetragonal	Pseudocubic	Tetragonal	Pseudocubic	Pseudocubic
Domains structures	Long-range FE domains	PNRs	Long-range FE domains	No long-range FE domains	No long-range FE domains
Slope of e_r vs. ln(f)	–	–56	–11	–21	–23
Frequency dependence of T_m	Weak	Weak		Strong	
Difference between T_m and T_B	~30 K	~240 K		~95 K	
Initial strain loop	–	Positive S_{irr}		Negative S_{irr}	

Figures

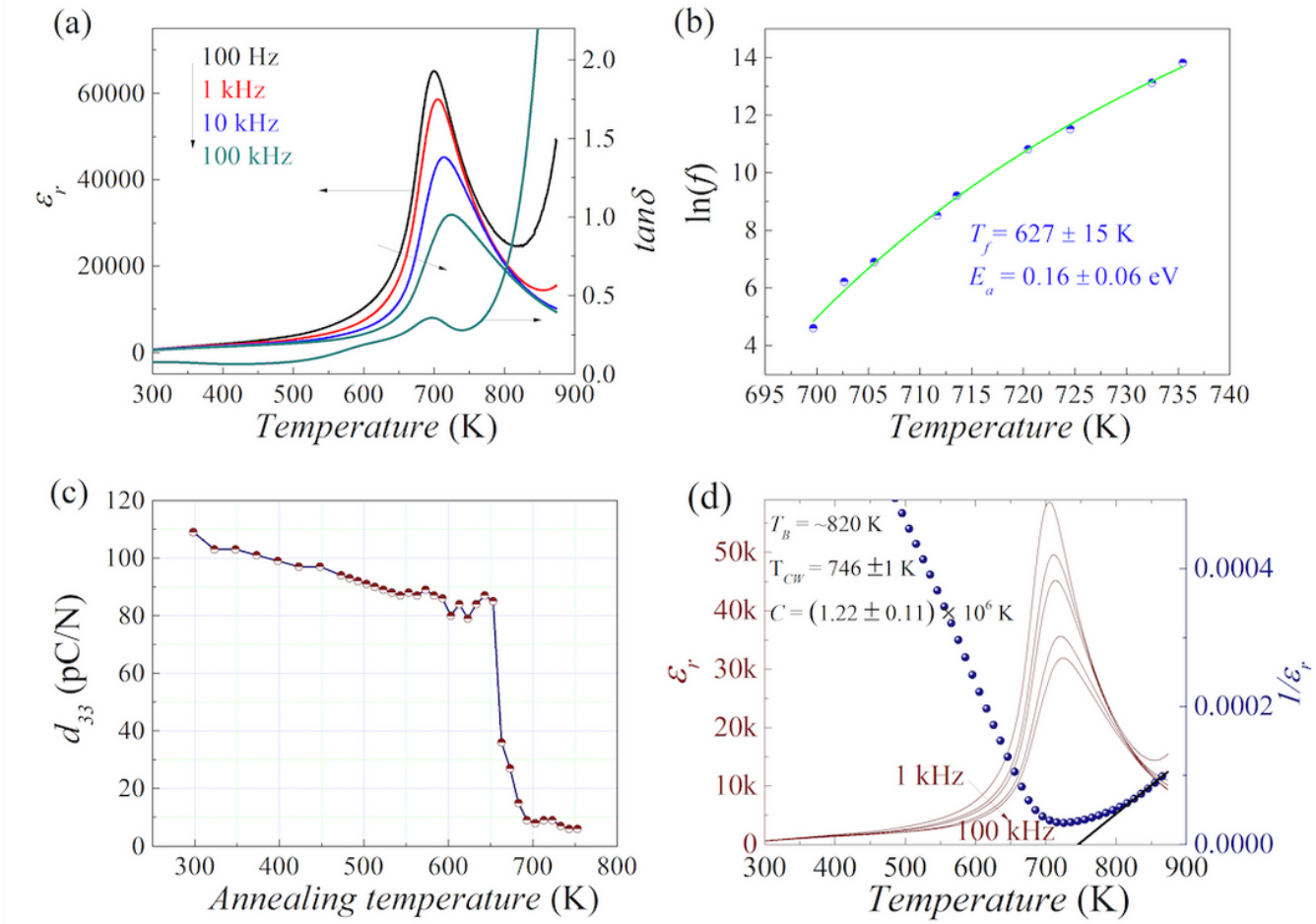

Figure 1

(a) Temperature dependence of relative permittivity (εr) and dielectric loss (tanδ) at selected frequencies, (b) Vogel-Fulcher law fitting, (c) relation of piezoelectric coefficient (d33) and annealing temperature and (d) Curie-Weiss law fitting of 0. 0.67BF–0.33BT.

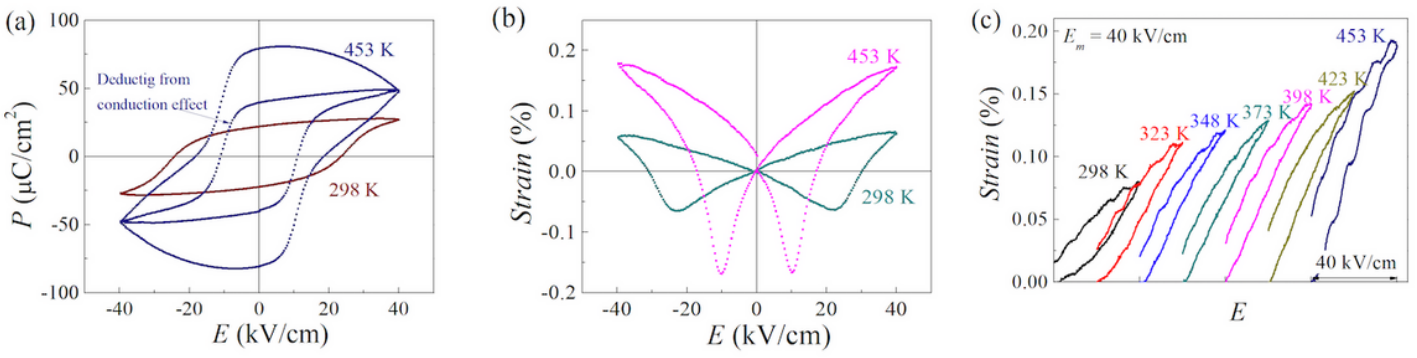

Figure 2

(a) polarization, (b) bipolar and (c) unipolar strain responses at various temperatures of 0. 0.67BF–0.33BT.

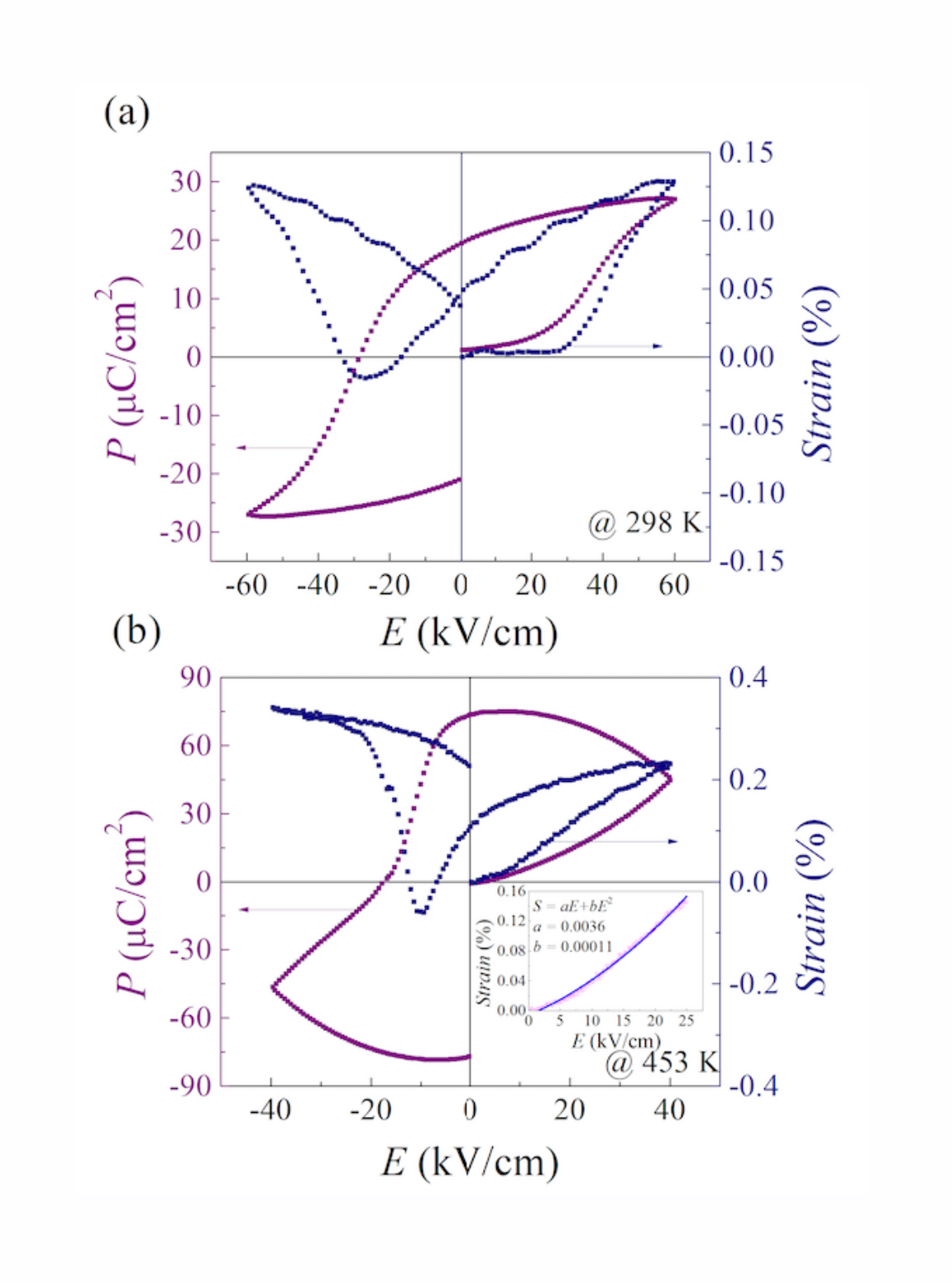

Figure 3

First-cycle ferroelectric hysteresis loops and electro-strain loops of 0. 0.67BF–0.33BT at (a) 298 K and (b) 453 K, inset of Fig. 3 (b) shows the fitting for the initial curve of the strain and electric field.

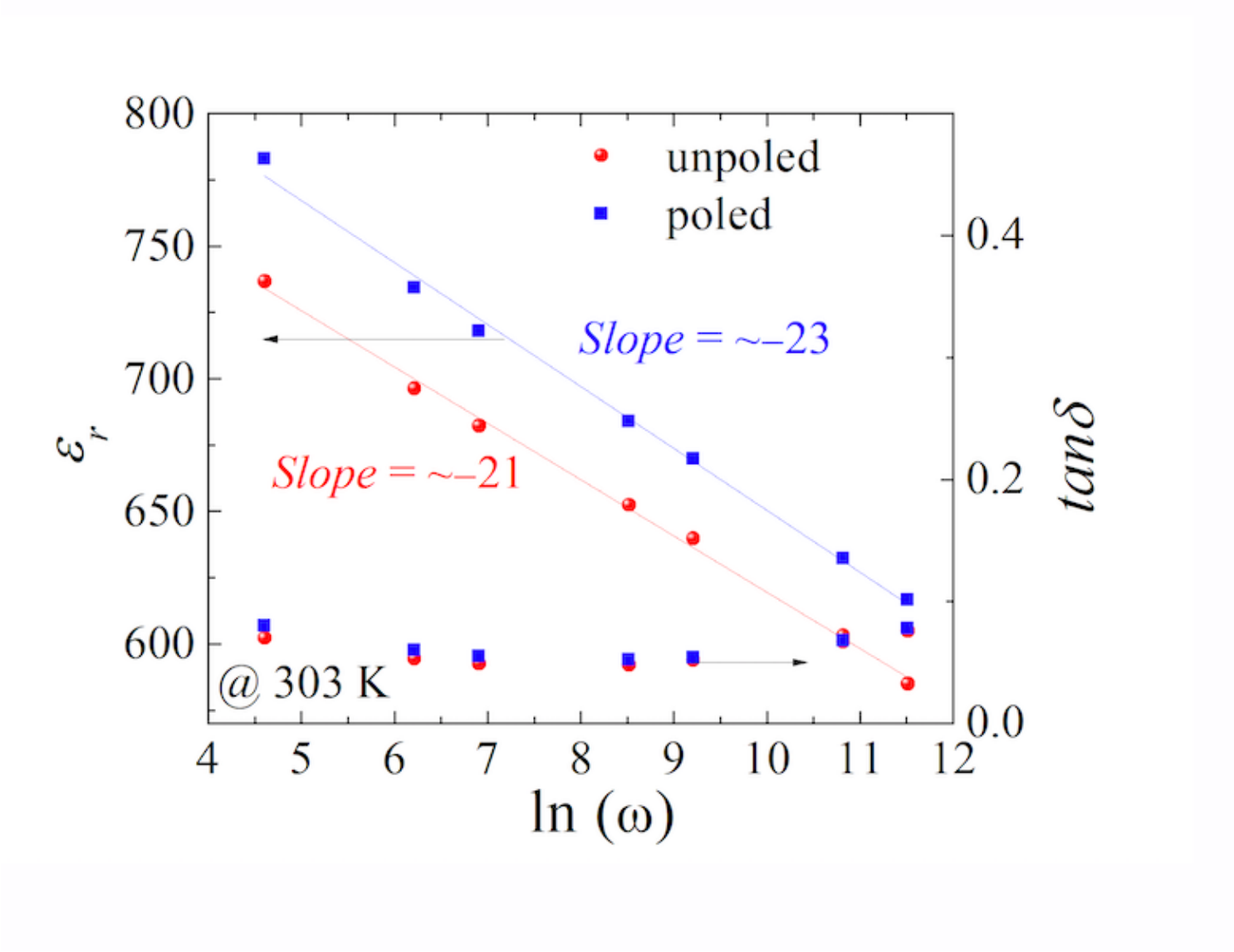

Figure 4

Poling effect on the frequency dependence of dielectric behaviors of 0.67BF–0.33BT

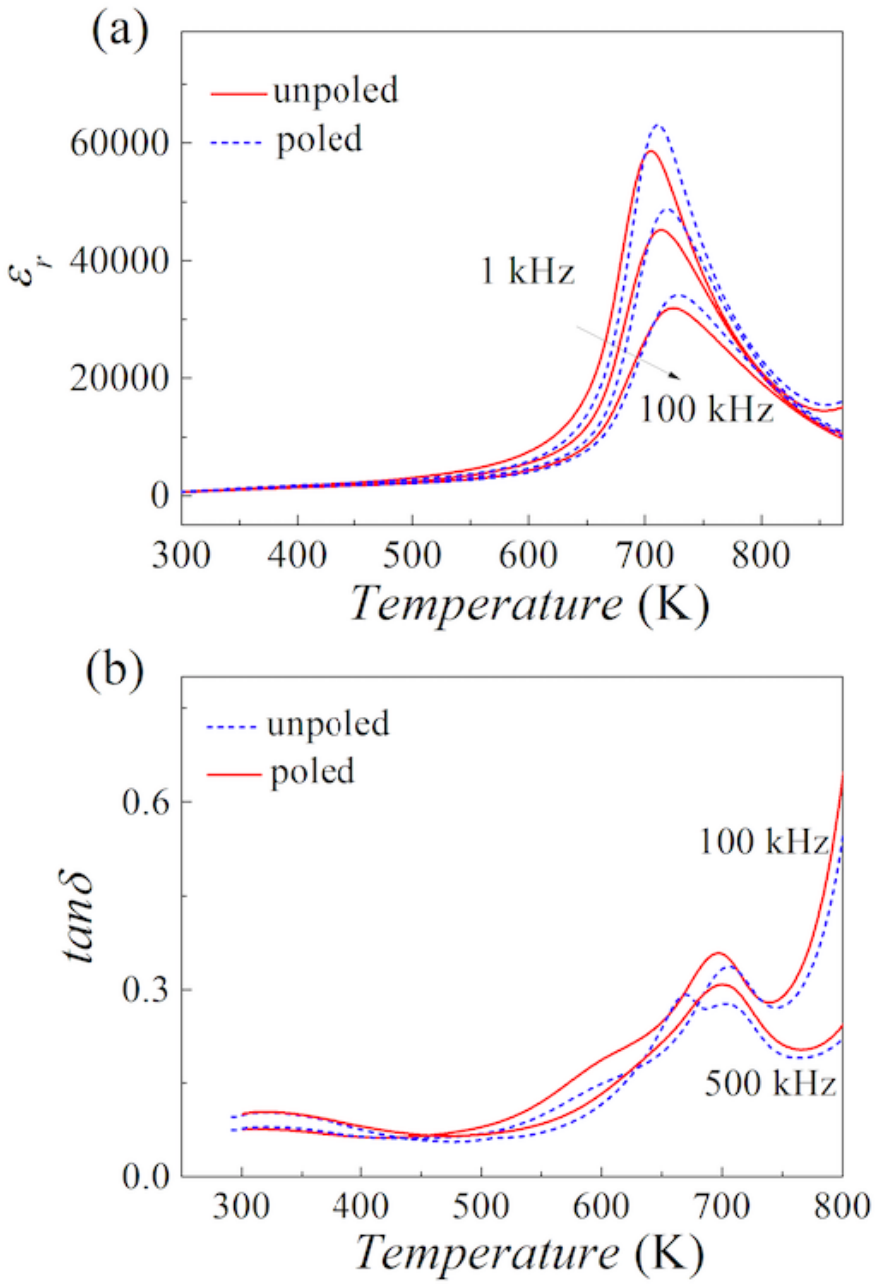

Figure 5

Poling effect on the temperature dependence of εr and tanδ of 0. 0.67BF−0.33BT

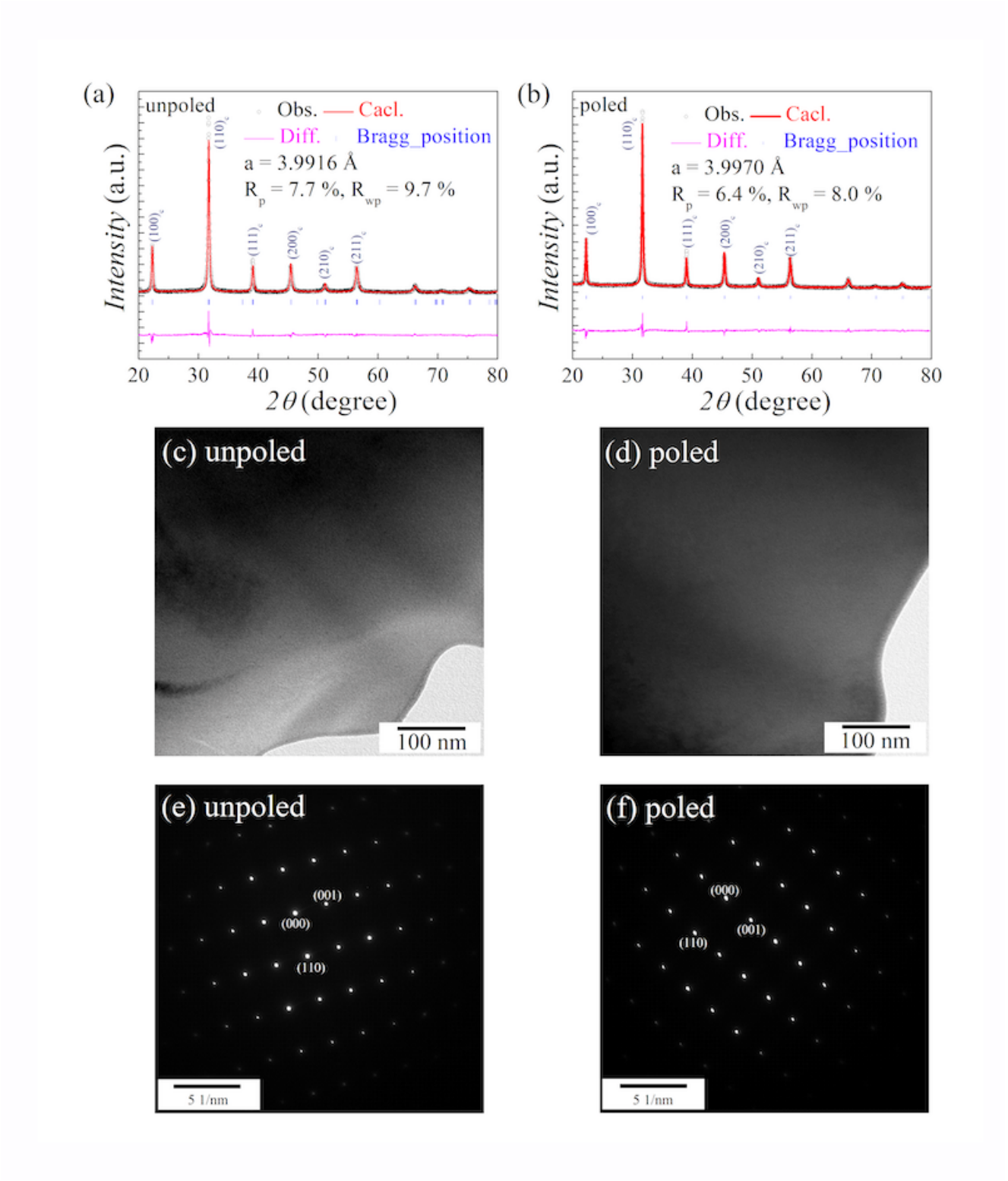

Figure 6

Rietveld fitted powder XRD patterns of (a) unpoled and (b) poled state, the black cycles represent the observed pattern, the red continuous line is correspond to the fitted pattern, the blue vertical bars point the Bragg peak positions, the magenta continuous line at the bottom represents the difference between the observed and fitted pattern. Poling effects on the (c), (d) bright-field images and (e), (f) SAED patterns.

Supplementary Files

This is a list of supplementary files associated with this preprint. Click to download.

- supportingmaterials.pdf